Conformational Dynamics of a Lipid-Interacting Protein: MD Simulations of Saposin B†

Daniel Stokeley,‡,§ Daniele Bemporad,‡,⊥ David Gavaghan,§ and Mark S. P. Sansom*,‡

Department of Biochemistry, University of Oxford, South Parks Road, Oxford OX1 3QU, U.K., Computing Laboratory, University of Oxford, Oxford OX1 3QD, U.K., and Johnson and Johnson Pharmaceutical Research and Development, Turnhoutseweg 30, 2340 Beerse, Belgium

Received July 5, 2007; Revised Manuscript Received September 12, 2007

ABSTRACT: Saposin B is a water soluble α-helical protein which can bind to membranes and extract selected lipids, especially cerebroside sulfates. The X-ray structure of saposin B is homodimeric. There are two conformations of the dimer in the crystal—one with a closed central cavity (the AB dimer) and one (the CD dimer) with a more open cavity. We have conducted a series of short (5 ns) molecular dynamics simulations of saposin B, starting from both the AB and CD conformations and with/without bound lipid and/or water molecules within the central hydrophobic cavity. The more open (CD) dimer showed greater conformational drift than the AB dimer. The conformational drift was also somewhat higher in the absence of bound lipid. Two more extended (30 ns) simulations of AB and CD dimers were performed and analyzed in terms of changes in intersubunit packing within the dimers. The AB dimer remained largely unchanged in conformation over the duration of the extended simulation. In contrast, the CD dimer underwent a substantial conformational change corresponding to a 'scissor' motion of the two monomers so as to compress the central cavity to a more closed conformation than that seen in the AB dimer structure. A H-bond between the Q53 and Y54 side chains of the α3 helices of the two opposing monomers seems to hold the dimer in this 'scissor-closed' conformation. We suggest that a cycle of conformational changes, expanding and compressing the central cavity of the saposin B dimer, may play a key role in facilitating lipid extraction from bilayers.

Proteins that interact with lipids are of considerable biomedical interest (*1*). A number of such proteins are able to interact with membranes so as to enable metabolism and/or transfer of lipids. The saposins are a family of soluble proteins, lacking enzymatic activity, that interact with lysosomal membranes (*2*). They are thought to act via binding to the surface of the membranes and then 'extracting' lipid molecules (*3*). More generally, the saposins are members of an extended family of saposin-like proteins (*4*), which have been implicated in a diverse range of membrane-related activities.

Saposin B (also known as the cerebroside sulfate activator) is one of the better characterized members of this family. It is a small (80 residues) nonenzymatic protein with a largely α-helical fold (*5*), related in structure to saposins A and C (*6*). Saposins are an essential component of the process that breaks down glycosphingolipids within the lysosome. Saposin B can extract cerebroside sulfates from lipid bilayers, solubilizing and presenting them to the arylsulphatase A which hydrolyzes the sulfate group to form galactosylceramide (*5*). Defects in the saposin B protein are associated with metachromic leukodystrophy, a neurodegenerative disease (*7*). Saposin B exhibits some degree of lipid selectivity (*7*, *8*) and also plays a role in lipid transport between membranes (*9*).

The X-ray structure of saposin B has been determined at 2.2 Å (*5*). The crystallographic unit cell of saposin B contains three structurally independent but sequence identical peptide chains (A, B, C) (*5*). Each chain (i.e., monomer) contains four α-helices, folded in an approximate L-shape with two antiparallel helices (α1 and α4, α2 and α3) forming each branch of the L. Two distinct homodimers are formed in the crystal (Figure 1). The first dimer is formed by chains A and B and thus is asymmetric. The second dimer, which is symmetric, is formed by C and D where D is a symmetry-related chain to C (by a twofold axis). In each dimer the two L-shaped monomers are wrapped around each other, forming a central hydrophobic cavity which, in the AB dimer, appears to contain a bound phospholipid molecule. Significantly, the cavity in the CD dimer is more open than that of the AB dimer. Based on comparison of the crystal structures of the AB and CD dimers, it has been suggested that a conformational transition of the dimer may play a key role in opening and closing the cavity to facilitate extraction of lipids from membranes (*5*).

The X-ray structures of saposins A and C have also been determined (*6*). Both saposins A and C are monomeric in their crystals, although there is evidence for dimer or trimer formation at low pH in the presence of detergent. Comparison

† Research in M.S.P.S.'s laboratory is supported by the BBSRC, the EPSRC, and the Wellcome Trust. D.S. was supported by an EPSRC studentship.

* To whom correspondence should be addressed. Phone: +44-1865-275371. Fax: +44-1865-275273. E-mail: mark.sansom@bioch.ox.ac.uk.

‡ Department of Biochemistry, University of Oxford.

§ Computing Laboratory, University of Oxford.

⊥ Johnson and Johnson Pharmaceutical Research and Development.

10.1021/bi701320a CCC: $37.00
Published on Web 11/06/2007

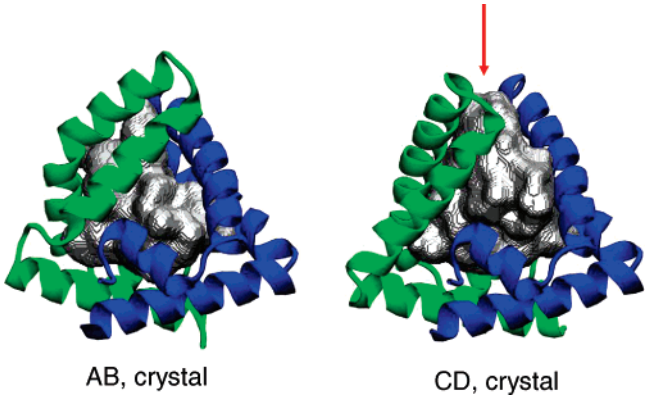

FIGURE 1: Crystal structures of saposin B, showing the (A) AB and the (B) CD dimers. In each case the protein subunits are colored blue (A or C) and green (B or D). The lining of the central cavity is shown as a gray surface. The arrow indicates the open entrance to the central cavity in the CD structure.

of the structures of monomeric saposins A and C with saposin B suggest that A and C correspond to a 'closed' form of B, in which the hydrophobic core of the protein has collapsed in on itself. Thus the X-ray structures indicate that the saposin dimer may undergo changes in conformation, which can alter the accessibility of the central cavity in the saposin B dimer. The saposin monomer is also able to adopt more than one conformation, as seen in, e.g., the NMR structure of saposin C in the absence/presence of detergent (*10*). Thus, a fuller understanding of the conformational dynamics of the saposin B dimer is required in order for us to understand the relation between structure and function of saposins.

Molecular dynamics (MD)[1] simulations provide a computational approach to exploring the conformational dynamics of proteins (*11*). In recent years, they have become of particular value as a tool for studying membrane proteins (*12*) and for characterization of proteins that bind fatty acids and lipids (*13*−*17*). In the current study we employ multiple MD simulations to explore the conformational dynamics of the saposin B dimer, extending the picture arising from analysis of the X-ray structures. The results of these simulations suggest a mechanism of conformational change of the saposin B dimer which may be related to its biological function.

METHODS

System Setup. The saposin B coordinates were taken from the Protein Data Bank (*18*), entry 1N69 (*5*). Ionization states of the side chains were the standard ones for pH 7. All protein models were simulated in a box of SPC water molecules (*19*), with sufficient counterions (sodium) added to keep the systems electrically neutral. The protein, waters, and the counterions were separately coupled to an external bath (*20*) with a weak coupling constant (0.1 ps). Electrostatic interactions were calculated with the particle mesh Ewald method (*21*, *22*) employing a grid spacing of ~1 $Å^{-1}$ and an interpolation order of 4. A cutoff of 12 Å was used for the real space portion of the Ewald sum and the Lennard-Jones interactions. The LINCS algorithm (*23*) was applied for constraining all covalent bonds, and the SETTLE algorithm (*24*) was used to maintain the geometry of the water molecules.

[1] Abbreviations: MD, molecular dynamics; PCA, principal components analysis; PE, phosphatidyl ethanolamine; RMSD, root mean square deviation; RMSF, root mean square fluctuation.

Table 1: Summary of Simulations

simulation	protein	lipid	cavity water	duration	Cα RMSD (Å)[a]
AB+l+cw	AB	+	+	3 + 5	2.0 (±0.1)
AB−l+cw	AB	−	+	3 + 5	3.8 (±0.1)
AB−l+cw30	AB	−	+	3 + 30	3.8 (±0.1)
AB+l−cw	AB	+	−	3 + 5	2.9 (±0.3)
AB−l−cw	AB	−	−	3 + 5	3.4 (±0.2)
CD+l+cw	CD	+	+	3 + 5	3.9 (±0.1)
CD−l+cw	CD	−	+	3 + 5	5.8 (±0.2)
CD−l+cw30	CD	−	+	3 + 30	6.0 (±0.3)
CD+l−cw	CD	+	−	3 + 5	4.5 (±0.4)
CD−l−cw	CD	−	−	3 + 5	4.5 (±0.3)

[a] RMSDs were averaged over the production phase (i.e., the latter 5 or 30 ns of the simulation) and are given ± standard deviation.

The downloaded crystal structure (*5*) included coordinates for chains A, B, and C plus crystallographic water molecules and a bound phosphatidyl ethanolamine (PE) molecule. The water molecules were retained in the initial structures used in the simulations. The second monomer of the CD dimer was generated by rotating C about a crystallographic twofold axis to yield coordinates for subunit D. This rotation was also applied to water molecules bound to C to yield those bound to D.

A PE lipid molecule was only present in the cavity of the AB dimer. To generate a lipid in the CD cavity, the CD dimer was superimposed onto the AB dimer (aligning only chains A and C) and the lipid position from the original AB structure was superimposed onto the CD dimer.

Simulation Protocol. MD simulations were performed with GROMACS 3.1.4 (*25*, *26*) (www.gromacs.org), using the GROMOS96 force field (*27*, *28*). All systems were first minimized using the steepest descent algorithm. Then the solvent was relaxed by performing a 50 ps MD simulation at 300 K with weak (force constant = 1000 kJ mol^{-1} nm^{-2}) positional restraints on the protein heavy (i.e., non-H) atoms. A series of six 10 ps MD simulations with no position restraints were carried out at 50, 100, 150, 200, 250, and 300 K, respectively, to gently heat the protein before the production simulations. The latter were 8 ns long (apart from two 30 ns simulations), and the first 3 ns were discarded as an equilibration period. Analysis of simulations used Gromacs, DSSP (*29*), Ligplot (*30*)), VMD (*31*), and Rastop (*32*).

RESULTS

Simulations and Stability. A summary of the simulations performed is provided in Table 1. Simulations of both the AB and CD dimer were performed in order to compare their conformational dynamics and, in particular, to explore any changes in the degree of opening/closure of the entrance to the cavity. We also performed simulations with/without water molecules initially in the central cavity and with/without a bound PE molecule in the cavity (see Methods for details). In this way we wished to probe the effect of the initial simulation setup on the conformational dynamics of the two dimers.

Initial measures of the conformational stability of the saposin B dimers were provided by DSSP (to analyze protein

secondary structure as a function of time; see Supporting Information, Figure S1) and by evaluation of Cα atom root-mean-square deviations (RMSDs) from their respective starting structures to probe overall conformational drift. In all of the simulations, DSSP analysis revealed that the protein secondary structure underwent only minor local fluctuations with no significant protein unfolding.

Analysis of the Cα RMSDs (Table 1; also see Supporting Information, Figure S2) reveals some interesting differences between the degree of conformational drift from the initial structure in the various simulations. Overall, the conformational drift is significantly less for simulations of the AB dimer (Cα RMSDs of 2 to 4 Å) than of the CD dimer (4 to 6 Å). Also of significance is the effect of the presence/absence of a bound PE molecule within the cavity of the dimer. Thus, in the absence of bound lipid ("−l" simulations) the Cα RMSD is consistently higher than in the presence of lipid ("+l" simulations). In contrast, the presence or absence of water molecules initially within the hydrophobic cavity did not seem to have a consistent effect on the overall conformational drift. On the basis of these analyses, the two "−l+cw" simulations were extended to 30 ns to enable further comparison of possible conformational changes. From these more extended simulations, it was clear that the difference in Cα RMSDs between the AB simulation (3.8 Å) and the CD simulation (6.0 Å) was maintained.

Protein Flexibility. To provide a more detailed insight into the nanosecond time scale flexibility of the protein at a local (i.e., residue-by-residue) level, we examined the root-mean-square fluctuations (RMSF) of individual residues (Figure 2). The overall patterns of fluctuations correlated with the crystallographic temperature factors, i.e., higher RMSFs for the interhelix loops. Of particular interest, and in general agreement with the RMSD analysis, those simulations performed *without* the lipid in the cavity showed greater fluctuations than those with the lipid. In particular, residues in the vicinity of residue 40 (at the end of helix α2, and close to mouth of the cavity), and to a lesser extent also the regions around residues 20 (the end of helix α1) and 60 (close to the end of α3), showed elevated RMSF values relative to the corresponding simulations with bound lipid. Also, the elevation of the RMSF (relative to the simulations with bound lipid) around residue 40 was more marked for the CD than for the AB simulations. To extend this analysis, a principal components analysis (*33*) (PCA) was performed on the equilibrated portion of the relevant trajectories. Results from the PCA agreed well with the RMSF analysis, in that the principal component contains the motion of the loop region around residue 40 (see below). Thus, the local flexibility around residue 40 appears to be significant and to be modulated by the presence/absence of bound lipid within the central cavity.

It has been suggested that the kink at residue Y54 of the B chain could be implicated in the binding mechanism of saposin B (*5*). Our simulations suggest that the kink angle in chain B was comparable to that of the other chains, i.e., the greater kink of chain B was not preserved over time during the simulations. However, it appears that the kink angles of both chains are more pronounced when a lipid is present in the binding pocket, in agreement with the experimental data (*5*) (see Supporting Information, Figure S3).

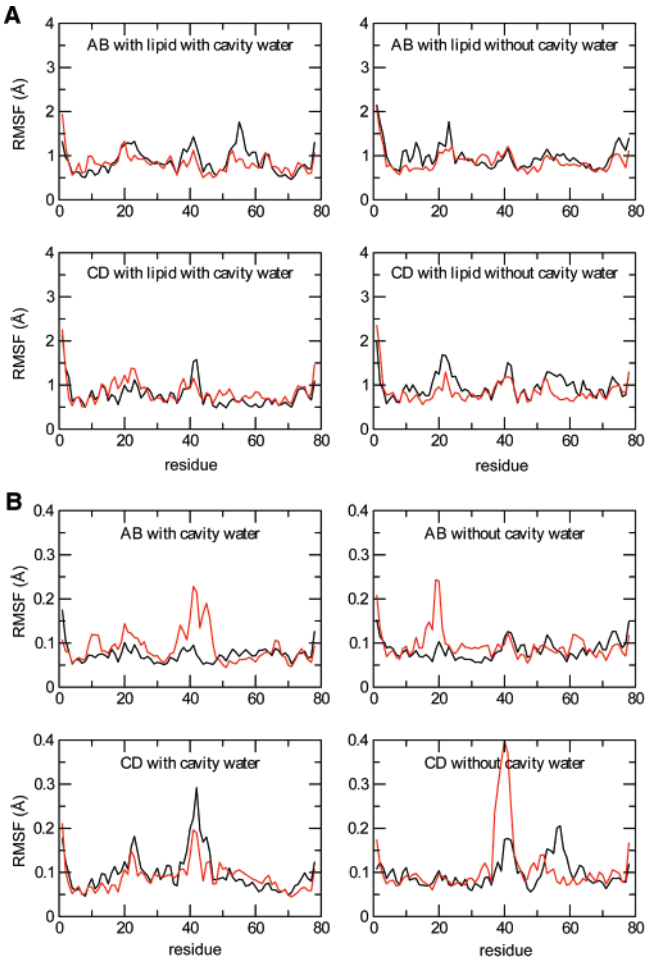

FIGURE 2: Root-mean-square fluctuation (RMSF) profiles of protein Cα atoms as a function of residue number during the production phase of the simulations (3−8 ns). (A) RMSF values for simulations with lipid present; (B) RMSF values for simulations without lipid. (Black lines: chains A and C; red lines: chains B and D.)

Distances between each pair of Cα atoms over the course of the simulation were calculated. The residues which showed the maximum deviation from their mean distance were P41 of one chain and the corresponding residue P41′ of the other chain, which correspond to the tops of the loops between α-helices at the entrance to the cavity. To understand how the motions of the rest of the protein correlated with the movement of these two residues, the correlation function defined in ref *34* was utilized. This specifies a correlation coefficient:

$$C_i = \frac{\langle (R_i(t) - \langle R_i \rangle)(d(t) - \langle d \rangle) \rangle}{\sqrt{\langle (R_i(t) - \langle R_i \rangle)^2 \rangle \langle (d(t) - \langle d \rangle)^2 \rangle}}$$

where d is the distance between P41:Cα and P41′:Cα and R_i is the coordinate of all the remaining Cα atoms in the protein. The C_i values projected onto the protein structure are shown in Figure 3. In the AB simulation, the motion of chain A is much more highly correlated than the motion of chain B, showing that it is chain A that is dictating the motion of the cavity entrance. Some motion can also be seen at the hinge point of chain B. For CD as anticipated the correlations are much more symmetrically distributed between the two chains. In both simulations it is evident that the highest correlations were with residues local to P41 and P41′. Thus

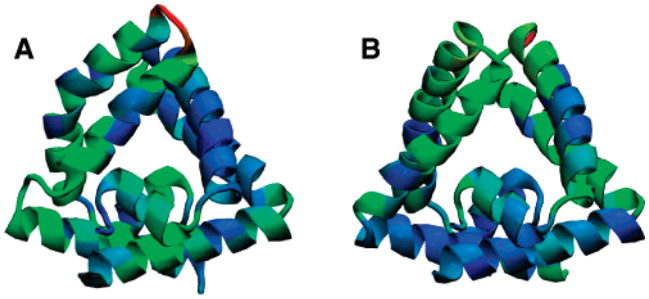

FIGURE 3: Correlations of motions with the P41:Cα (chain A or C) and P41:Cα (chain B or D) interchain distance for (A) the AB dimer (simulation AB−l+cw) and (B) the CD dimer (simulation CD−l+cw). The structure is colored on the correlation coefficient (C_i, see main text) such that red = high C_i and blue = low C_i.

it is evident that local flexing (as seen in, e.g., the RMSF profiles) at the hinge of the 'L' (i.e., the loop around residue 40) correlates with the dimensions of the 'gate' at the mouth of the central cavity. This suggests it is worthwhile to investigate possible changes in the 'gate' dimensions in more detail.

The Cavity and the Entrance: Conformational Changes. We have also examined the entrance to the protein cavity as defined by the top of the α2/α3 loop connecting the two α-helices including five residues on either side (i.e., 11 Cα atoms on each chain). The distance between the mean positions of both sets of 11 Cα atoms, d_{LL}, thus provides a measure of the size of the cavity entrance. The cavity width thus defined is shown as a function of time (Figure 4A) for the two −l+cw30 simulations. For the AB dimer, the initial (X-ray) d_{LL} value is ∼15 Å. In the corresponding simulation, there is a small rapid initial increase, followed by fluctuations around the same value, indicating only a minor change from the X-ray structure. For the CD dimer, over the first nanosecond, d_{LL} increases from ∼24 Å (in the X-ray structure) to ∼30 Å. It is clear that the CD dimer has a consistently greater entrance width than AB. There is a significant initial increase in d_{LL} for the CD dimer, and substantial fluctuations occur later in the simulation. The same increase to d_{LL} ∼ 30 Å occurs in the short CD−l+cw simulation, again within ∼1 ns. Interestingly, in the corresponding simulation with bound lipid (CD+l+cw; data not shown) d_{LL} remains close to the value in the crystal structure. Thus it would seem that the presence of a lipid molecule in the cavity prevents the substantial conformational change in CD (as can also be seen from the RMSD values in Table 1).

To investigate the pathway for lipids/water molecules into/out of the cavity, snapshots of the protein at maximum and minimum cavity opening widths (i.e., min-d_{LL} and max-d_{LL}) were saved. In Figure 5A,B the snapshots are of the CD−l+cw simulation in its min-d_{LL} and max-d_{LL} conformations. It can be seen that the latter conformation is achieved by a 'scissoring' motion of the dimer, rather than a simple 'opening/closing' of the cavity entrance. PCA analysis of the simulations (Figure 5C) indicates that such a scissoring motion corresponds to the principal eigenvector.

Interactions with Water and with Lipid. In all cases where the simulation was started with water within the (hydrophobic) cavity, the water was rapidly expelled and dropped to the level seen in those simulations started without cavity water molecules. The water occupancy of cavities in proteins shows a complex dependence on cavity hydrophobicity and

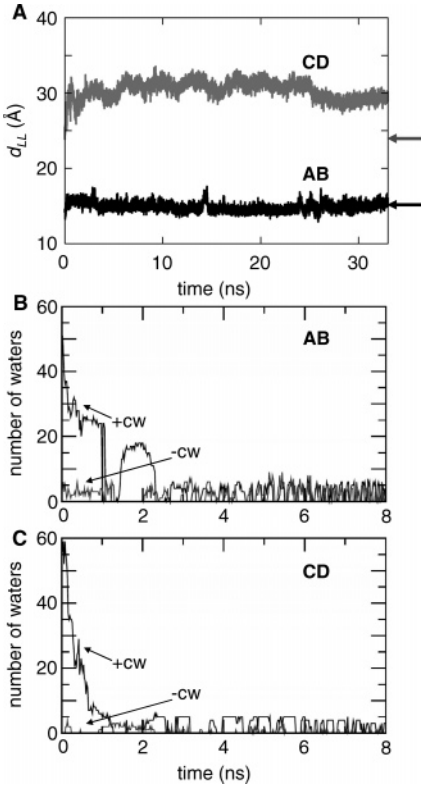

FIGURE 4: (A) Loop−loop distances (d_{LL}) (defined as between the centers-of-mass of the Cα atoms of residues 36−46 on each chain) as functions of time for the AB−l+cw30 (black line) and CD−l+cw30 (gray line) simulations. The two arrows on the right-hand side indicate the corresponding values of d_{LL} in the X-ray structure. Also shown is the number of cavity waters vs time for (B) simulations AB−l+cw (black line) and AB−l−cw (gray line) and for (C) simulations CD−l+cw (black line) and CD−l−cw (gray line).

solvent conditions (*35*). This suggests that the hydrophobic lining of the cavity will favor partitioning of the lipid molecules into the protein binding pocket.

To investigate the binding properties of the lipid, LIGPLOT (*30*) was applied to a series of snapshots (saved every 50 ps) from each simulation. It has been suggested that R38 may be involved in the binding of cerebroside sulfate to saposin B (*5*). However, the hydrogen bond between R38 and the PE is short-lived in the simulation (Table 2). Instead, the main primary residues involved in H-bonds with the lipid (PE) headgroup are Y50 and Y54. Additionally there are a large number of hydrophobic contacts between the lipid tails and the hydrophobic residues lining the cavity of the protein.

Interchain Contacts. A more detailed analysis of the conformational change seen in the saposin B simulations was provided by analysis of interchain contact matrices (Figure 6). From visualization of the simulations it appears that saposin B does not fluctuate between the AB dimer and CD dimer form, but rather that the open (CD) form collapses and scissors into a conformation where the cavity entrance as defined by d_{LL} (*5*) becomes wider. To try to understand what causes the two dimers to behave differently, analysis was undertaken on the interchain contacts of both dimers.

In this analysis, if two residues are within 4 Å of each other, then they are considered to be in contact. In Figure 6A,B we consider the contacts in the crystal alongside the results from the corresponding −l+cw simulations. In the

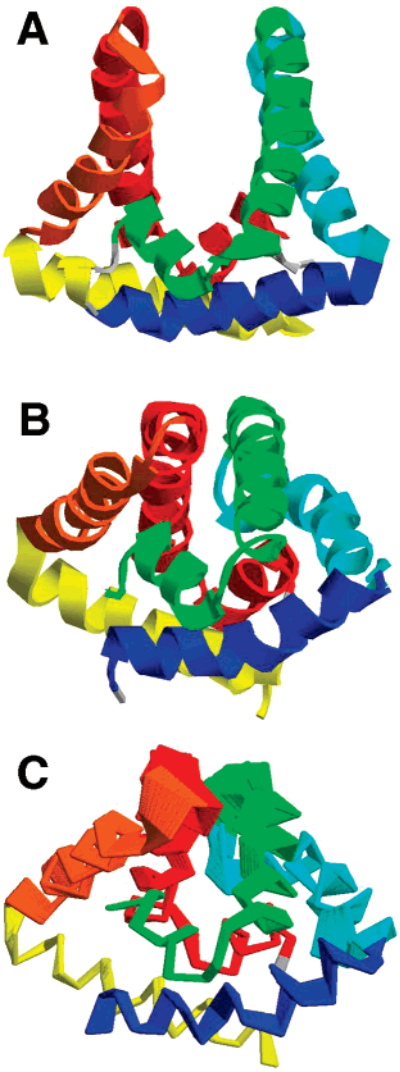

FIGURE 5: Structures from the CD−l+cw simulation showing the (A) min-d_{LL} and (B) max-d_{LL} conformations. (C) Results of PCA of the CD−l+cw simulation, showing the two extreme projections along a trajectory on the average structure and 20 frames interpolated between them. In each of the three cases, the view is approximately perpendicular to the vertical 2*x* axis, and the protein is colored on an RGB color scale (i.e., blue, cyan, green for the helices of subunit C and yellow, orange, red for subunit D).

Table 2: H-Bonded Contacts between Saposin B and Lipid[a]

residue	appearance in simulations (/8)	% presence
E35	2	9
R38	3	5
G40	1	6
Y50	2	25
Y54	3	21
Q60	2	8
H64	2	12
E69	3	5

[a] The residues identified by LIGPLOT (*30*) as forming H-bonds with the lipid are analyzed. The number of simulations (out of the (four simulations × two chains) that were performed with the lipid present) in which a residue formed H-bonds to PE and the percentage of simulation snapshots (saved every 50 ps) in which the H-bond was present are listed.

AB structure a cluster of contacts appears in the crystal in the cavity entrance region (denoted by the yellow boxed region), and these are largely maintained during the simulation. This cluster of contacts is hydrophobic, involving the side chains of M43 and I46 (see Figure 7A).

The corresponding results of the interchain contact analysis of the CD dimer (Figure 6C,D) reveal a rather different picture. In the crystal there are no residues in contact range within the region around the cavity entrance, and in fact there are few residue contacts stabilizing the (tertiary structure) of the protein at all. In the CD−l+cw simulation (Figure 6D), the residues around the cavity entrance do *not* form contacts during the simulation. Instead, contacts are made outside of the entrance region, by antiparallel packing together of the α3 helices from the two monomers. So although the entrance has become wider, in terms of the distance between the ends of the two hairpins, the potential space for a lipid may in fact have decreased due to the angle of collapse of the protein and the new contacts formed.

This analysis alongside visualization of the simulations suggests that the residues around the cavity entrance that form contacts in the AB dimer (e.g., M43 and I46) may be responsible for the conformational stability of the protein in this form. The CD dimer lacks these contacts and is therefore less conformationally stable and seems to collapse into a further, more stable, structure. This conclusion is drawn from the pattern of contacts in the α3/α3 contact region that appear highly conserved during the simulation of the CD dimer but are absent from the crystal. The RMSD results support this, showing a rise during the first 3 ns, followed by a plateau. In particular, it seems that the side chains of Q53 and Y54 may form a H-bond which acts as a 'latch', holding the CD dimer in the new conformation (Figure 7B). Thus in the CD−l+cw30 simulation this H-bond is present, intermittently, throughout the simulation (see Supporting Information, Figure S4), whereas in the AB−l+cw30 simulation, this H-bond is not formed at all.

CONCLUSIONS

Our simulations suggest a marked degree of conformational instability (on the ∼10 ns time scale) in the saposin B dimer when it is removed from the crystal environment. This correlates with, e.g., recent NMR data on saposin C (*10*), which are also consistent with multiple conformations, albeit in the monomer, such that there is a switch between 'closed' and 'open' forms dependent on the presence/absence of detergent (SDS). This idea of intrinsic conformational malleability is further supported by crystallographic studies of saposins A and C (*6*, *36*).

Combining this information with the results of our simulations we may, albeit tentatively, suggest a model for saposin B dynamics (Figure 8). In this model, the X-ray structure of the CD dimer represents the most 'open' form of the dimer. This may close, as seen in the X-ray structure of the AB dimer, to form a discrete central hydrophobic cavity. This may (in the absence of lipid in the cavity) close further in a 'scissoring' motion conformational change as seen in the CD simulations.

We may explore this model a little further in terms of the protein interactions and solvation energies of the different states portrayed in Figure 8. Thus, in terms of solvation energy, as we progress from the X-ray structure of the CD dimer to that of the AB dimer to the CD simulations, there is a decrease in the strength of protein/solvent interactions,

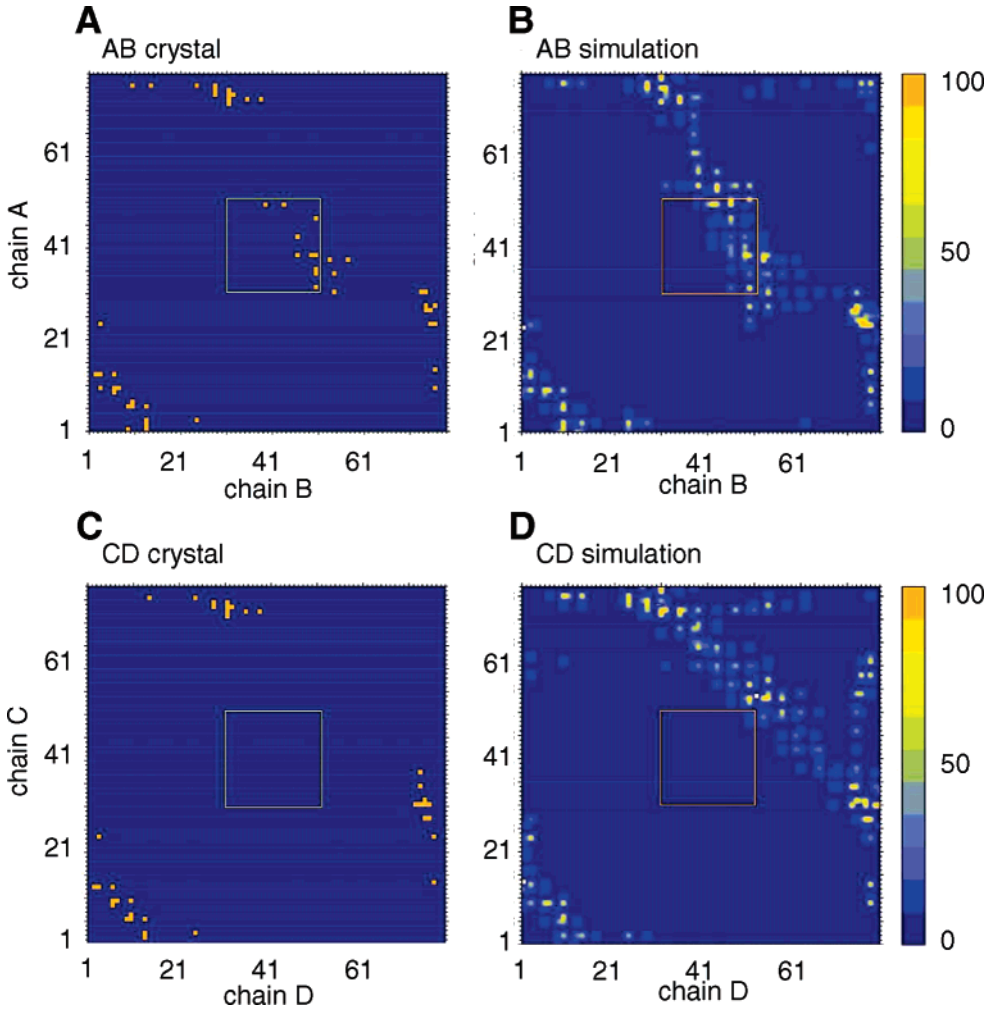

FIGURE 6: Analysis of interchain contacts of the AB (A, B) and CD (C, D) dimers in the crystal (A, C) and simulations (B, D; for the AB−l+cw and CD−l+cw simulations). In each case the color scale is from blue (0% contacts) to orange (100% contacts, where the normalization is onto a percentage of simulation time). The cutoff distance for a contact is 4 Å, and for the simulations, contacts are averaged over a 5 ns (i.e., post-equilibration) period.

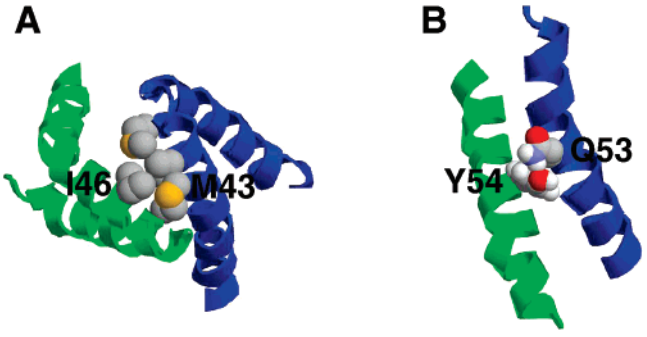

FIGURE 7: (A) Hydrophobic contacts at the mouth of the cavity in the AB crystal structure, showing the side chains of M43 and I46. (B) The H-bond between the side chains of Q53 and Y54 which forms a 'latch' between the two α3 helices in the scissor-closed structure seen in the CD simulations.

reflecting the formation of the closed hydrophobic cavity. At the same time there is an increase in the strength of protein intramolecular interactions, mainly at the level of electrostatic rather than van der Waals interactions. (Further details are provided in the Supporting Information, Table S1.)

It is tempting, but perhaps premature, to speculate on the relationship of this proposed cycle of conformational changes to the function of saposin B. It has been suggested that the conformational changes of saposins may be related to their

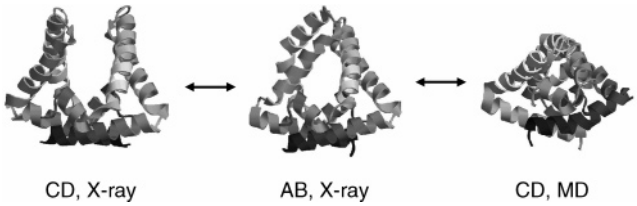

FIGURE 8: Schematic diagram of the proposed pathway for conformational change of the saposin dimer from an 'open' structure (the CD dimer from the X-ray structure), through an intermediate structure (the AB dimer from the X-ray structure), to a 'scissor-closed' structure (a CD max-d_{LL} conformation).

ability to bind to, and extract lipids from, lipid bilayers (*3*). The scissor-closed (CD simulation) conformation is held closed by a Q53/Y54 H-bond. It is likely that this H-bond can be broken upon interaction with a lipid bilayer, reversing the sequence of conformational changes and thus opening up the cavity to facilitate extraction of a lipid molecule from the bilayer.

One question which does arise is whether the two forms of the dimer (i.e., AB and CD) observed in the crystal are present in solution. It would be of interest to explore the relationship between the crystal and solution structures by, e.g., running MD simulations of the crystal unit cell (see, e.g., ref *37*) and comparing the degree of con-

formational overlap with the corresponding MD simulations in solution.

One should remain aware of the limitations of the current simulation. The main limitation is that the relatively short timescales available to atomistic MD simulations do not allow for full sampling of multiple conformations of membrane-interacting proteins (*38*, *39*), even though some information concerning interdomain conformational changes in relatively simple water soluble proteins may be obtained (*40*−*42*). Thus, although single conformational transitions (e.g., 'open' to 'closed') may be sometimes observed in a simulation, it is not possible to fully sample conformational equilibria by direct simulation on a nanosecond time scale. In the present case, much longer simulations would probably be required in order to observe, e.g., a transition of the scissor-closed conformation back to the open cavity (i.e., as seen in the CD X-ray structure) conformation.

Thus, to more fully understand the nature of the dynamic interactions of saposins with lipid bilayers, it may be necessary to employ multiscale models. Thus, elastic network models enable us to address large scale conformational changes in proteins (*43*−*45*), coarse-grained models allow one to explore the interactions of proteins and membranes (*46*, *47*), and atomistic simulations allow details of protein, ligand, and water conformational dynamics to be explored. Using such a multiscale approach should enable us in the future to define the role of dynamic conformational events in saposin function.

SUPPORTING INFORMATION AVAILABLE

Figure S1, a secondary structure plot for simulation AB−l+cw; Figure S2, RMSD of Cα atoms over time for the AB and CD simulations; Figure S3, showing the kink angle of chain B as a function of time in simulations AB−l+cw and AB+l+cw; Figure S4, hydrogen bonds between the latch-forming Q53 and Y54 side chains; and Table S1, summarizing intraprotein and protein solvation energies. This material is available free of charge via the Internet at http://pubs.acs.org.

REFERENCES

1. de Kruijff, B. e. (2005) Lipid-protein interactions, *Biochim. Biophys. Acta 1666*, 1−290.
2. Bruhn, H. (2005) A short guided tour through functional and structural features of saposin-like proteins, *Biochem. J. 389*, 249−257.
3. Alattia, J. R., Shaw, J. E., Yip, C. M., and Prive, G. G. (2006) Direct visualization of saposin remodelling of lipid bilayers, *J. Mol. Biol. 362*, 943−953.
4. Munford, R., Sheppard, P., and O'Hara, P. (1995) Saposin-like proteins (SAPLIP) carry out diverse functions on a common backbone structure, *J. Lipid Res. 36*.
5. Ahn, V. E., Faull, K. F., Whitelegge, J. P., Fluharty, A. L., and Prive, G. G. (2003) Crystal structure of saposin B reveals a dimeric shell for lipid binding, *Proc. Natl. Acad. Sci. U.S.A. 100*, 38−43.
6. Ahn, V. E., Leyko, P., Alattia, J. R., Chen, L., and Prive, G. G. (2006) Crystal structures of saposins A and C, *Protein Sci. 15*, 1849−1857.
7. Fluharty, C., Johnson, J., Whitelegge, J., Faull, K., and Fluharty, A. L. (2001) Comparative lipid binding study on the cerebroside sulfate activator (saposin B), *J. Neurosci. Res. 63*, 82−89.
8. Remmel, N., Locatelli-Hoops, S., Breiden, B., Schwarzmann, G., and Sandhoff, K. (2007) Saposin B mobilizes lipids from cholesterol-poor and bis(monoacylglycero)phosphate-rich membranes at acidic pH, *FEBS J. 274*, 3405−3420.
9. Faul, K., Whitelegge, J., Higginson, J., To, T., Johnson, J., Krutchinsky, A., Standing, K., Waring, A., Stevens, R., Fluharty, C., and Fluharty, A. L. (1999) Cerebroside sulfate activator protein (saposin B): chromatographic and electrospray mass spectrometric properties, *J. Mass. Spectrom. 34*, 1040−1054.
10. Hawkins, C. A., de Alba, E., and Tjandra, N. (2005) Solution structure of human saposin C in a detergent environment, *J. Mol. Biol. 346*, 1381−1392.
11. Adcock, S. A., and McCammon, J. A. (2006) Molecular dynamics: survey of methods for simulating the activity of proteins, *Chem. Rev. 106*, 1589−1615.
12. Ash, W. L., Zlomislic, M. R., Oloo, E. O., and Tieleman, D. P. (2004) Computer simulations of membrane proteins, *Biochim. Biophys. Acta 1666*, 158−189.
13. Likic, V. A., and Prendergast, F. G. (1999) Structure and dynamics of the fatty acid binding cavity in apo rat intestinal fatty acid binding protein, *Protein Sci. 8*, 1649−1657.
14. Likic, V. A., Juranic, N., Macura, S., and Prendergast, F. G. (2000) A "structural" water molecule in the family of fatty acid binding proteins, *Protein Sci. 9*, 497−504.
15. Molnar, F., Norris, L. S., and Schulten, K. (2000) Simulated (un)-binding of arachidonic acid in the cyclooxygenase site of prostaglandin H-2 synthase-1, *Prog. React. Kinet. Mech. 25*, 263−298.
16. Friedman, R., Nachliel, E., and Gutman, M. (2005) Molecular dynamics simulations of the adipocyte lipid binding protein reveal a novel entry site for the ligand, *Biochemistry 44*, 4275−4283.
17. Friedman, R., Nachliel, E., and Gutman, M. (2006) Fatty acid binding proteins: Same structure but different binding mechanisms? Molecular dynamics simulations of intestinal fatty acid binding protein. *Biophys. J. 90*, 1535−1545.
18. Berman, H. M., Westbrook, J., Feng, Z., Gilliland, G., Bhat, T. N., Weissig, H., Shindyalov, I. N., and Bourne, P. E. (2000) The Protein Data Bank, *Nucl. Acids Res. 28*, 235−242.
19. Berendsen, H. J. C., Postma, J. P. M., van Gunsteren, W. F., and Hermans, J. (1981) Interactions models for water in relation to protein hydration, in *Intermolecular Forces*, Reidel, Dordrecht.
20. Berendsen, H. J. C., Postma, J. P. M., van Gunsteren, W. F., DiNola, A., and Haak, J. R. (1984) Molecular dynamics with coupling to an external bath, *J. Chem. Phys. 81*, 3684−3690.
21. Darden, T., York, D., and Pedersen, L. (1993) Particle mesh Ewald - an N.log(N) method for Ewald sums in large systems, *J. Chem. Phys. 98*, 10089−10092.
22. Essmann, U., Perera, L., Berkowitz, M. L., Darden, T., Lee, H., and Pedersen, L. G. (1995) A smooth particle mesh Ewald method, *J. Chem. Phys. 103*, 8577−8593.
23. Hess, B., Bekker, H., Berendsen, H. J. C., and Fraaije, J. G. E. M. (1997) LINCS: A linear constraint solver for molecular simulations, *J. Comput. Chem. 18*, 1463−1472.
24. Miyamoto, S., and Kollman, P. A. (1992) Settle - an analytical version of the Shake and Rattle algorithm for rigid water models, *J. Comput. Chem. 13*, 952−962.
25. Lindahl, E., Hess, B., and van der Spoel, D. (2001) GROMACS 3.0: a package for molecular simulation and trajectory analysis, *J. Mol. Model. 7*, 306−317.
26. van der Spoel, D., Lindahl, E., Hess, B., Groenhof, G., Mark, A. E., and Berendsen, H. J. (2005) GROMACS: fast, flexible, and free, *J. Comput. Chem. 26*, 1701−1718.
27. van Gunsteren, W. F., Kruger, P., Billeter, S. R., Mark, A. E., Eising, A. A., Scott, W. R. P., Huneberger, P. H., and Tironi, I. G. (1996) *Biomolecular Simulation: The GROMOS96 Manual and User Guide*, Biomos & Hochschulverlag AG an der ETH Zurich, Groningen and Zurich.
28. Scott, W. R. P., Hunenberger, P. H., Tironi, I. G., Mark, A. E., Billeter, S. R., Fennen, J., Torda, A. E., Huber, T., Kruger, P., and van Gunsteren, W. F. (1999) The GROMOS biomolecular simulation program package, *J. Phys. Chem. A 103*, 3596−3607.
29. Kabsch, W., and Sander, C. (1983) Dictionary of protein secondary structure: pattern-recognition of hydrogen-bonded and geometrical features, *Biopolymers 22*, 2577−2637.
30. Wallace, A. C., Laskowski, R. A., and Thornton, J. M. (1995) LIGPLOT: a program to generate schematic diagrams of protein-ligand interactions, *Protein Eng. 8*, 127−134.
31. Humphrey, W., Dalke, A., and Schulten, K. (1996) VMD - Visual Molecular Dynamics, *J. Mol. Graphics 14*, 33−38.

32. Sayle, R. A., and Milner-White, E. J. (1995) RasMol: Biomolecular graphics for all, *Trends Biochem. Sci. 20*, 374−376.
33. Amadei, A., Linssen, A. B. M., and Berendsen, H. J. C. (1993) Essential dynamics of proteins, *Proteins: Struct. Funct. Genet. 17*, 412−425.
34. Bui, J., Henchman, R., and McCammon, J. (2003) The dynamics of ligand barrier crossing inside the acetylcholinesterase gorge, *Biophys. J. 85*, 2267−2272.
35. Collins, M. D., Hummer, G., Quillin, M. L., Matthews, B. W., and Gruner, S. M. (2005) Cooperative water filling of a nonpolar protein cavity observed by high-pressure crystallography and simulation, *Proc. Natl. Acad. Sci. U.S.A. 102*, 16668−16671.
36. Schultz-Heienbrok, R., Remmel, N., Klingenstein, R., Rossocha, M., Sandhoff, K., Saenger, W., and Maier, T. (2006) Crystallization and preliminary characterization of three different crystal forms of human saposin C heterologously expressed in Pichia pastoris, *Acta Crystallogr. F 62*, 117−120.
37. Bond, P. J., Faraldo-Gómez, J. D., Deol, S. S., and Sansom, M. S. P. (2006) Membrane protein dynamics and detergent interactions within a crystal: a simulation study of OmpA, *Proc. Natl. Acad. Sci. U.S.A. 103*, 9518−9523.
38. Faraldo-Gómez, J. D., Forrest, L. R., Baaden, M., Bond, P. J., Domene, C., Patargias, G., Cuthbertson, J., and Sansom, M. S. P. (2004) Conformational sampling and dynamics of membrane proteins from 10-nanosecond computer simulations, *Proteins: Struct. Funct. Bioinf. 57*, 783−791.
39. Grossfield, A., Feller, S. E., and Pitman, M. C. (2007) Convergence of molecular dynamics simulations of membrane proteins, *Proteins: Struct. Funct. Bioinf. 67*, 31−40.
40. Pang, A., Arinaminpathy, Y., Sansom, M. S. P., and Biggin, P. C. (2005) Comparative molecular dynamics - similar folds and similar motions? *Proteins: Struct. Funct. Bioinf. 61*, 809−822.
41. Pantano, S., Zaccolo, M., and Carloni, P. (2005) Molecular basis of the allosteric mechanism of cAMP in the regulatory PKA subunit, *FEBS Lett. 579*, 2679−2685.
42. Pentikäinen, U., Pentikäinen, O. T., and Mulholland, A. J. (2007) Cooperative symmetric to asymmetric conformational transition of the apo-form of scavenger decapping enzyme revealed by simulations, *Proteins: Struct. Funct. Bioinf.* (in press), doi:10.1002/prot.21540.
43. Bahar, I., Atilgan, A. R., and Erman, B. (1997) Direct evaluation of thermal fluctuations in proteins using a single-parameter harmonic potential, *Fold. Des. 2*, 173−181.
44. Atilgan, A. R., Durell, S. R., Jernigan, R. L., Demirel, M. C., Keskin, O., and Bahar, I. (2001) Anisotropy of fluctuation dynamics of proteins with an elastic network model. *Biophys. J. 80*, 505−515.
45. Eyal, E., Yang, L., and Bahar, I. (2006) Anisotropic Network Model: systematic evaluation and a new web interface. *Bioinformatics 22*, 2619−2627.
46. Bond, P. J., and Sansom, M. S. P. (2006) Insertion and assembly of membrane proteins via simulation, *J. Am. Chem. Soc. 128*, 2697−2704.
47. Bond, P. J., Holyoake, J., Ivetac, A., Khalid, S., and Sansom, M. S. P. (2007) Coarse-grained molecular dynamics simulations of membrane proteins and peptides, *J. Struct. Biol. 157*, 593−605.

BI701320A